Inverted-S Antenna With Wideband Circular Polarization and Wide Axial Ratio Beamwidth

Long Zhang, Steven Gao, *Senior Member, IEEE*, Qi Luo, *Member, IEEE*, Paul R. Young, *Senior Member, IEEE*, Wenting Li, and Qingxia Li, *Member, IEEE*

Abstract—A novel broadband circularly polarized (CP) antenna with wide axial ratio (AR) beamwidth is proposed. It is composed of two curved arms shaped like an inverted "S." The mechanisms of wideband CP operation and wide AR beamwidth are explained. To validate the concept, a prototype at C-band is manufactured and measured. Experimental results confirm that the antenna achieves an impedance bandwidth of 63% and a CP bandwidth of 42%. Furthermore, maximum AR beamwidth of 140° is achieved and wide AR beamwidth can be maintained in a frequency bandwidth of 35% in nearly all elevation planes. In addition, the antenna has the advantage of being easily extended to arrays. A four-element array using the proposed antenna is investigated through both simulations and experiments, and achieves 60% CP bandwidth and wide AR beamwidth. The proposed inverted-S antenna can realize wide CP bandwidth and wide AR beamwidth, and can easily form wideband CP arrays.

Index Terms—Broadband antenna, circular polarization, wide axial ratio (AR) beamwidth, wideband array.

I. INTRODUCTION

CIRCULARLY polarized (CP) antennas are widely deployed in various wireless systems due to their advantages of the mitigation of multipath fading, the reduction of "Faraday rotation," and the immunity of polarization mismatching between transmitting and receiving antennas [1]. Extensive research work on improving the axial ratio (AR) bandwidth of CP antennas has been reported, as the traditional microstrip patches with perturbations exhibit less than 5% bandwidth [2]. Dual-feed technique and 90° hybrid were used to increase the CP bandwidth [3]. Other antennas, such as stacked patches [4], slot antenna [5], and magnetoelectric dipole [6] are also good candidates for wideband CP operation.

Besides improving the AR bandwidth, widening the AR beamwidth of CP antennas was received increasing interest due to their applications in global navigation satellite systems (GNSSs) [7] and wide-angle CP beam-scanning array [8]. Several researches on this topic were reported including a square-ring slotted patch antenna [9], an asymmetric microstrip antenna with integrated circular-patches [10], and an elliptical vertical patch antenna backed by an elliptical

air cavity [11]. Although these CP antennas can achieve more than 120° AR beamwidth, their AR bandwidths are smaller than 5%. For some applications, such as covering all GNSS bands, these antennas may not applicable.

To meet the system requirement of large bandwidth, normally the antenna needs to be designed as either multiband or wideband. The multiband CP antennas with wide AR beamwidth in each working band can be found in [12]–[14]. In [12], a multibranch crossed dipole was presented with more than 110° AR beamwidth. Stacked cone-patches were used to achieve dual-band operation and over 110° AR beamwidth [13]. A dual-frequency dual CP patch antenna with orthogonal and offset-centered slots was reported in [14], which realized right-hand circular polarization (RHCP) and left-hand circular polarization (LHCP) at two different bands with more than 160° AR beamwidth. However, for high data rate satellite communications, it is always desirable to have a wideband antenna with wide AR beamwidth especially for the receivers.

Despite the importance of wideband CP antennas with wide AR beamwidth, there are few reported researches. Two pairs of parallel dipoles were orthogonally placed in a square contour and were excited in phase quadrature to acquire wide AR beamwidth when the space between the parallel dipoles was appropriately chosen [15]. The AR bandwidth of this antenna is from 1.52 to 1.65 GHz (8.2%) and 126° AR beamwidth is achieved at 1.6 GHz. However, the AR beamwidth decreases when frequency shifts away from 1.6 GHz. A stacked patch antenna with 10.2% CP bandwidth and 140° AR beamwidth was presented in [16]. Likewise, the AR beamwidth is measured at only 2.4 GHz and the AR beamwidths at other frequency points within the working band are not provided. In [17], a wideband magnetoelectric dipole which has 33% AR bandwidth and 85° AR beamwidth within the AR passband in the two main planes was reported. Stable wide angular CP radiation could also be observed in [18], where a crossed dipole was loaded with a magneto-electric dipole to realize good CP performance. In [18], 27.7% AR bandwidth was achieved and over 165° AR beamwidth could be realized from 1.45 to 1.7 GHz (15.8%) in the two main planes. Although the antenna presented in [17] and [18] can achieve wideband CP radiation with wide angular CP coverage in the two main planes, it is not clear whether wide AR beamwidths can be maintained in other elevation planes. Moreover, these antennas have complicated structures, which make them difficult to be implemented in wideband CP arrays.

In this paper, a novel inverted S-shaped CP antenna with a simple configuration is presented, which achieves wide

Fig. 1.   Geometry of the proposed antenna.

TABLE I
ANTENNA PARAMETERS (mm)

L_1	L_2	W_1	W_2	W_3	W_4	W_5	H_1	H_2
80	90	45	8	1.77	2.46	0.8	18	14
H_3	H_4	H_5	H_6	H_7	R_1	R_2	R_3	R_4
21.5	11.5	6.23	2	30	15	12.5	12	10

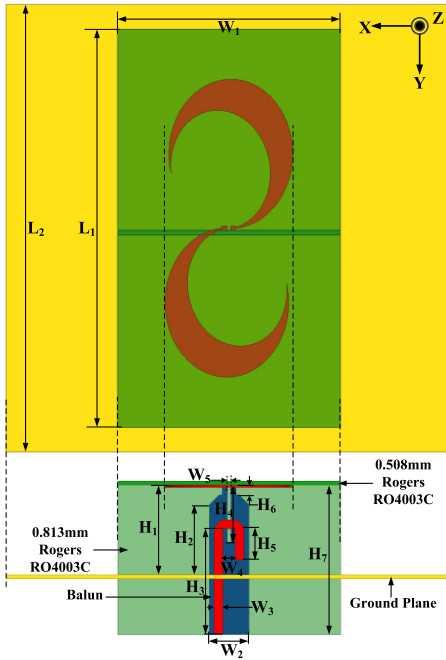Fig. 2.   Detailed geometry of the curved arm.

CP bandwidth and wide AR beamwidth simultaneously. Stable wide angular CP radiation characteristics are maintained in a wide frequency range in the *xoz* plane. In other elevation planes, the AR beamwidths are wider than the half power beamwidths (HPBWs). Compared with other reported antennas, the proposed antenna achieves a wider CP bandwidth and a more stable AR beamwidth within the operational bandwidth. Moreover, it can be easily extended to a wideband CP array with wide AR beamwidth, which is also discussed in this paper.

This paper is organized as follows. Section II introduces the antenna configuration and operational principles of wide angular CP radiation. Section III presents the simulation results and measurement results of the proposed antenna as well as the comparison with other reported antennas. Section IV presents a linear array consisting of the proposed antenna element and the results of this array. The conclusion is given in Section V.

II. ANTENNA CONFIGURATION AND OPERATIONAL PRINCIPLES

A. Antenna Configuration

The configuration and geometry dimensions of the proposed antenna are shown in Fig. 1. As shown, the antenna consists of two curved arms and is printed on the bottom layer of a 0.508 mm thick Rogers RO4003C substrate with a size of $W_1 \times L_1$. To feed the antenna, an integrated balun, which transforms the unbalanced microstrip feed to balanced slot line feed, is utilized. The balun is printed on both layers of a 0.813 mm thick Rogers RO4003C substrate which has a size of $W_1 \times H_7$. An $L_2 \times L_2$ sized ground plane is placed below the antenna with a distance of H_1, which is mainly used to achieve directional radiation.

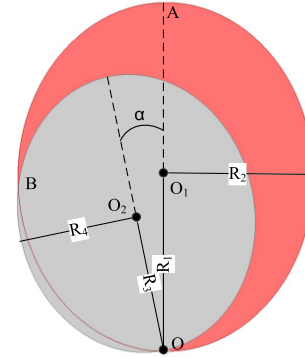The curved arm can be obtained through cutting a bigger ellipse by a smaller rotated ellipse, as shown in Fig. 2. This method is inspired by [19], where two concentric semicircles are used to form a vortex slot. As can be seen from Fig. 2, the bigger ellipse has a major axis radius R_1 and minor axis radius R_2 while the smaller ellipse's major and minor axis radius is R_3 and R_4, respectively. The smaller ellipse is counterclockwise rotated along point O with an angle of α and then it is subtracted from the bigger ellipse.

Table I gives the detailed antenna parameters. Besides, the rotation angle α is 10°. The lengths of the outer curve and inner curve are around 65 and 52 mm equaling to about $1.8\lambda_g$ and $1.4\lambda_g$ at the center frequency 5 GHz, which provide enough traveling paths for a traveling wave current flowing along the curved arm. The distance between the antenna and the ground plane (H_1) is chosen to be 18 mm to achieve maximum AR bandwidth. Meanwhile, the antenna gain can also be maintained at a reasonable value at this height. The ground plane size ($L_2 \times L_2$) is determined by taking into consideration of the performance of AR and radiation patterns. Generally, the AR bandwidth degrades but the back lobe gets decreased with larger L_2. The size of the ground plane is chosen to be 90 mm × 90 mm to achieve wide AR bandwidth and good radiation patterns.

B. Operational Principle of Circularly Polarized Radiation

To explain the operational principle of CP radiation, the surface current distribution on the curved arms at different time slots is shown in Fig. 3. As shown, the null area of the surface current is propagating along the curved arms, which is similar to the phenomenon observed in [20]. It is reported in [20] that a traveling wave current is realized along the equiangular strip and aperture edge. Different to [20], in this design the traveling wave current is excited along the curved arms even without any ground plane or cavity, which simplifies the fabrication and makes the presented antenna a better candidate for the array application. Furthermore, the proposed antenna exhibits wide AR beamwidth characteristic which is not observed in [20].
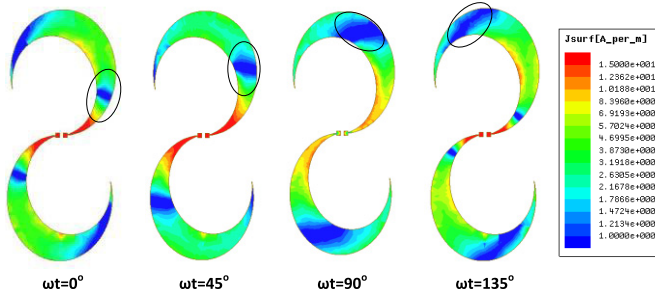
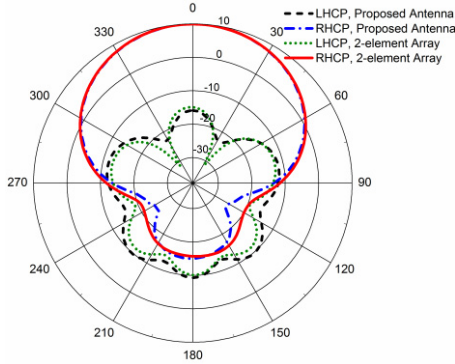Fig. 3.   Surface current on curved arms at different time slots.

Fig. 4.   Radiation patterns of the proposed antenna and the two-element array in *xoz* plane.

C. Mechanism of Wide Angular CP Radiation

Considering that the antenna consists of two curved arms fed out of phase, the far-field radiation of the proposed antenna can be synthesized using a two-element array. To validate this assumption, a two-element array was simulated and each curved arm is fed by a lumped port like a horizontal monopole, with 180° phase difference between the two ports.

For a fair comparison of the radiated electric field, the distance between the ground plane and the two-element array is kept 18 mm, the same as the height of the proposed antenna. The proposed antenna is fed by a lumped port to eliminate the influence of the balun. Fig. 4 shows the comparison of radiation patterns in RHCP and LHCP components between the proposed antenna and the two-element array at 4.7 GHz in the *xoz* plane. As shown, the far-field radiation between the proposed antenna and the two-element array is nearly the same. The agreement of the radiation patterns can also be observed at other frequencies and different elevation planes. Therefore, it is reasonable to deem the proposed antenna as a two-element array as shown in Fig. 5.

The radiated fields of the proposed antenna can then be obtained by vector summing of the fields radiated by each element (curved arm). As shown in Fig. 5, P_1 and P_2 denote the phase center of each element, respectively. Because the element 2 is acquired through rotating element 1 by 180° at the origin point O, the points P_1, P_2, and O are in a line. Denoting the distance between P_1 and P_2 by d and the angle between the line P_1OP_2 and axis X by φ_c, the spatial phase delay of the two elements in *xoz* plane can then be represented by

$$\delta = k_0 d \cos \varphi_c \sin \theta \qquad (1)$$

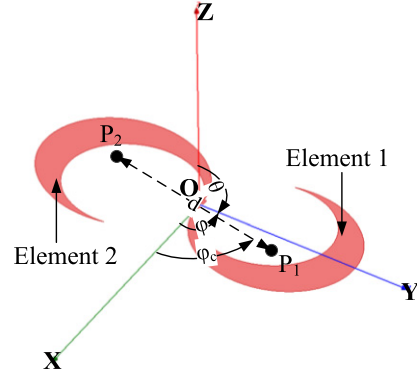where k_0 is the wavenumber in free space. For an elliptically

Fig. 5.   Geometrical arrangement of two-element array.

polarized antenna, the radiated electric field of element 1 can be written by [21]

$$\overrightarrow{E_1}(\theta, \varphi) = a(\theta, \varphi)\overrightarrow{e_\theta} + b(\theta, \varphi)\overrightarrow{e_\varphi} e^{j\frac{\pi}{2}}. \qquad (2)$$

Here, $a(\theta, \varphi)$ and $b(\theta, \varphi)$ are the amplitude of the two orthogonal unit vectors $\overrightarrow{e_\theta}$ and $\overrightarrow{e_\varphi}$, which are functions of θ and φ. For a qualitative analysis, the total field in *xoz* plane is deduced while the fields in other planes can also be derived by using different spatial phase delays between the two elements. As element 2 is axisymmetric to element 1, the radiated field of element 2 in *xoz* plane can be written as follows:

$$\overrightarrow{E_2}(\theta, 0) = -\overrightarrow{E_1}(\theta, \pi) = -\overrightarrow{E_1}(-\theta, 0). \qquad (3)$$

Here, the negative sign stems from the physical rotation angle π which results in a reverse direction of the electric field. The total electric field in *xoz* plane is given by

$$\overrightarrow{E_t}(\theta, 0) = \overrightarrow{E_1}(\theta, 0) + \overrightarrow{E_2}(\theta, 0)e^{j\pi}e^{j\delta}. \qquad (4)$$

The $e^{j\pi}$ component in (4) comes from the feeding phase difference π. Substituting (2) and (3) into (4) which can be rewritten as

$$\begin{aligned} \overrightarrow{E_t}(\theta, 0) &= \overrightarrow{E_1}(\theta, 0) + \overrightarrow{E_1}(-\theta, 0)e^{j\delta} \\ &= [a(\theta, 0) + a(-\theta, 0)e^{j\delta}]\overrightarrow{e_\theta} \\ &\quad + [b(\theta, 0) + b(-\theta, 0)e^{j\delta}]\overrightarrow{e_\varphi} e^{j\frac{\pi}{2}}. \end{aligned} \qquad (5)$$

Equation (5) indicates that the total field $\overrightarrow{E_t}$ in the *xoz* plane equals to the summation of field $\overrightarrow{E_1}(\theta, 0)$ and $\overrightarrow{E_1}(-\theta, 0)e^{j\delta}$. The physical insight of (5) is that the total field $\overrightarrow{E_t}$ originates from two elliptically polarized fields while the phase difference between them is δ. Due to the asymmetric radiation pattern to z-axis of each element, $\overrightarrow{E_1}(-\theta, 0)$ does not equal to $\overrightarrow{E_1}(\theta, 0)$ for a given elevation angle θ (except for $\theta = 0$). Denoting the AR of $\overrightarrow{E_1}(\theta, 0)$ by $AR_1(\theta)$ and the AR of $\overrightarrow{E_1}(-\theta, 0)$ by $AR_2(\theta)$, then

$$AR_2(\theta) = AR_1(-\theta) = a(-\theta, 0)/b(-\theta, 0). \qquad (6)$$

Also, $AR_2(\theta) \neq AR_1(\theta)$ except for $\theta = 0$. According to (5), for a given θ, the AR of the total field $\overrightarrow{E_t}$ is determined by AR_1, AR_2, and δ. Since $AR_2(\theta) \neq AR_1(\theta)$, it gives the possibility to realize a total field with a better AR_t ($AR_t < AR_1$ or AR_2).
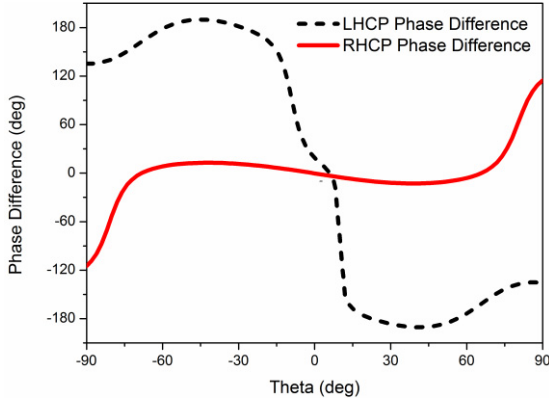
Fig. 6. Phase differences of RHCP and LHCP component between the two elements at 4.7 GHz in the *xoz* plane.
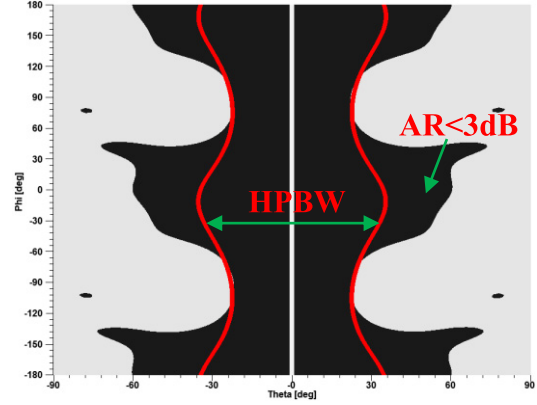

Fig. 7. AR and HPBW of the proposed antenna at 4.7 GHz.

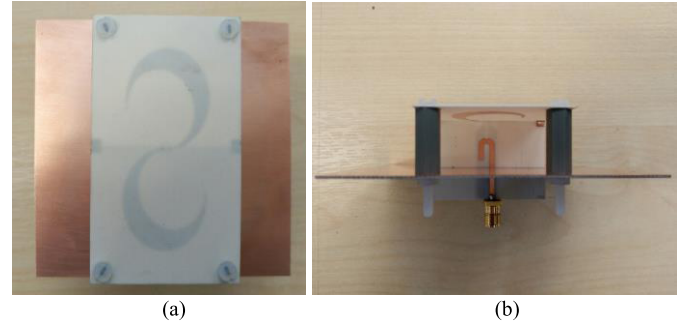Fig. 8. Prototype of the proposed antenna. (a) Top view. (b) Side view.

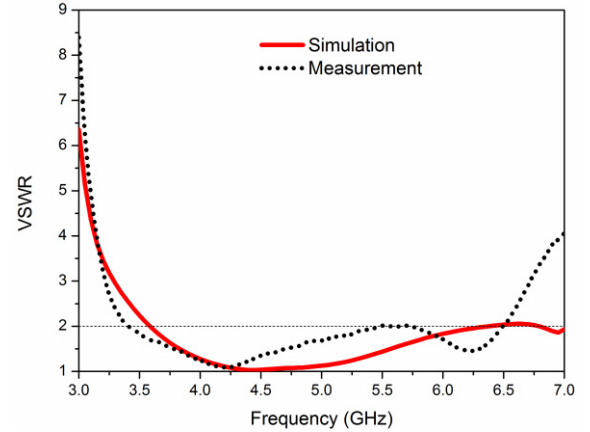Fig. 9. Simulated and measured VSWR of the proposed antenna.

To give a more visualized explanation, the phase differences of the RHCP and LHCP electric field component between the two elements in the *xoz* plane is shown in Fig. 6. For an easier comparison, element 2 is fed with an 180° phase difference to element 1. The far-field RHCP component phase difference is calculated by $\text{Phase}_{\text{RHCP,element 1}} - \text{Phase}_{\text{RHCP,element 2}}$ while the phase difference of LHCP component is calculated by $\text{Phase}_{\text{LHCP,element 1}} - \text{Phase}_{\text{LHCP,element 2}}$.

As shown in Fig. 6, the phase difference of the RHCP component (co-pol component) is around 0° from −70° to 70° angular range. This means that the RHCP components of the two elements are nearly in phase and can be superposed in a wide angular range. Meanwhile, the phase difference of the LHCP component (cross-pol component) is around −180° from 15° to 70° angular range and around 180° from −15° to −70° angular range. The LHCP components of the two elements are therefore canceled by each other in the angular range of 15° to 70° and −15° to −70°. As the RHCP component of the two-element array gets enhanced and the LHCP component gets decreased in a wide angular range, the AR improves in a wide angular range and wide angular CP radiation can be achieved.

From (5), the fields of two elements will be superposed in phase at broadside direction ($\theta = 0$). However, the phase difference of LHCP component is slightly larger than 0°. This phase error may be caused by the mutual coupling between the two elements. It is worth pointing out that these equations can also be applied to the "S" shaped antenna which radiates LHCP wave.

Fig. 7 shows the simulated AR and HPBW of the proposed antenna (without balun) in the upper hemisphere area at 4.7 GHz, which are obtained by using Ansys HFSS 15. The dark area denotes the region where the AR is smaller than 3 dB and the HPBW is bounded by the two red curves. Fig. 7 clearly demonstrates that the AR beamwidths in each elevation planes are larger than the HPBWs. The decrease of the AR beamwidth is along with the decrease of HPBW, leading to a wide AR beamwidth covering HPBW in the whole upper hemisphere.

III. RESULTS AND DISCUSSION

A. Antenna Prototype and VSWR

The prototype of the proposed antenna is shown in Fig. 8. As shown, a coaxial connector is connected to the end of the balun to feed the antenna. Four plastic pillars are used to support an 18 mm air gap between the antenna and the ground plane.

The simulated and measured VSWR of the proposed antenna is shown in Fig. 9. As can be seen, the measured impedance bandwidth (VSWR < 2) is from 3.4 to 6.5 GHz (63%). Compared with the simulated VSWR, the measured result is slightly shifted to lower frequency, which is caused by fabrication and measurement errors.
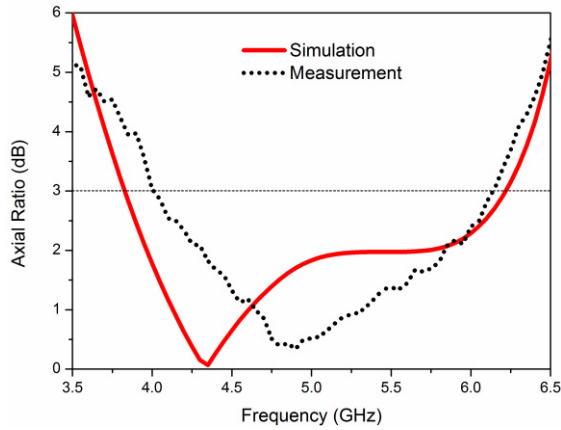
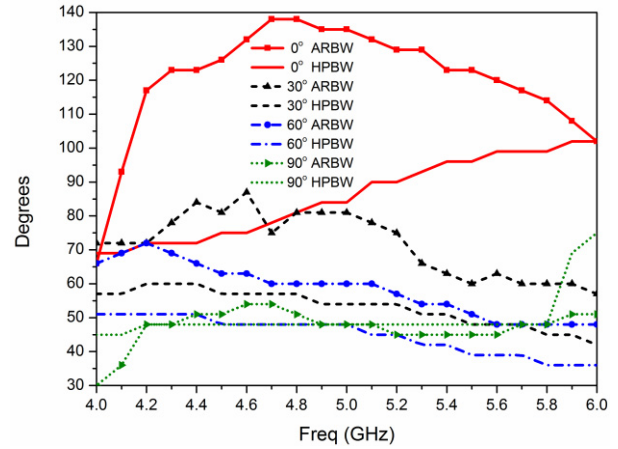Fig. 10.   Simulated and measured AR bandwidth of the proposed antenna.

Fig. 11.   Simulated and measured AR beamwidth in the *xoz* plane at different frequencies.

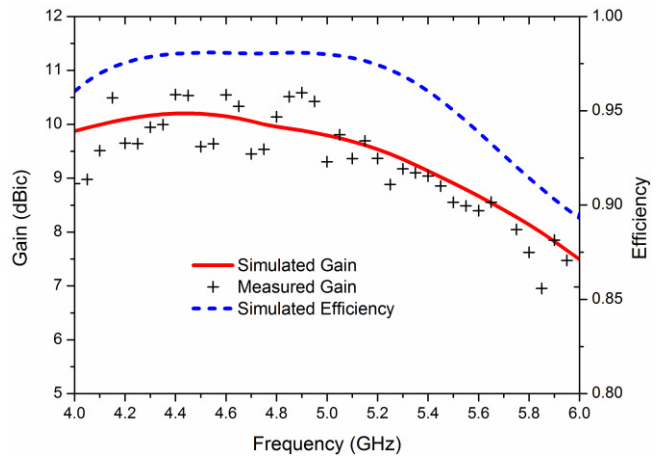Fig. 12.   Measured AR beamwidths and HPBWs in different cutting planes.

Fig. 13.   Antenna gain and simulated efficiency.

B. Axial Ratio Bandwidth

The AR bandwidth of the proposed antenna is shown in Fig. 10, which indicates the AR values in the broadside direction.

The measured AR bandwidth (AR < 3 dB) is from 4 to 6.15 GHz, results in a fractional bandwidth of 42%. Different to the simulated AR, the frequency of measured minimum AR point is shifted to a higher frequency which is around 5 GHz.

C. Axial Ratio Beamwidth

As aforementioned, the proposed antenna exhibits stable wide AR beamwidth apart from its wide AR bandwidth. The stable wide AR beamwidth of the proposed antenna not only rests on its wide AR beamwidth in the symmetric plane (*xoz* plane) but also lies in its AR beamwidths in other cutting planes, which are wider than HPBWs.

Fig. 11 shows the simulated and measured AR beamwidth in the *xoz* plane at different frequency points. As shown, the measured AR beamwidths in the *xoz* plane are 117°, 138°, and 123° at 4.2, 4.8, and 5.4 GHz, respectively. In line with the measured AR bandwidth shown in Fig. 10, the measured AR in other elevation angles is smaller than the simulated AR at higher frequencies, which also verifies the shifting of

minimum AR point to a higher frequency. The difference between the measurement and simulation results may come from the fabrication and measurement errors. It is also observed that the AR beamwidth is asymmetric to $\theta = 0°$, which is different to the symmetric AR beamwidth observed in Fig. 7. This asymmetry is caused by the integrated balun which has an asymmetric microstrip line to $\theta = 0°$ direction. Although the radiation of this microstrip line is small, it still introduces different influences to the CP radiation in different elevation angles θ [22].

To give an understanding of the AR beamwidths in other cutting planes and the comparison between the AR beamwidths and HPBWs, the values of measured AR beamwidths and measured HPBWs in planes $\varphi = 0°$, 30°, 60°, 90° are shown in Fig. 12. As can be seen, in elevation planes $\varphi = 0°$, 30°, 60°, the AR beamwidths are larger than the HPBWs from 4 to 6 GHz. However, in the $\varphi = 90°$ plane, the AR beamwidth is slightly smaller than the HPBW at some frequency points. As the value of AR is determined by the RHCP and LHCP component, slightly increase of cross-pol (LHCP) component makes the AR larger than 3 dB and results in a narrower AR beamwidth. In spite of this, the measured results still indicate that the proposed antenna can achieve a wide angular CP radiation in the
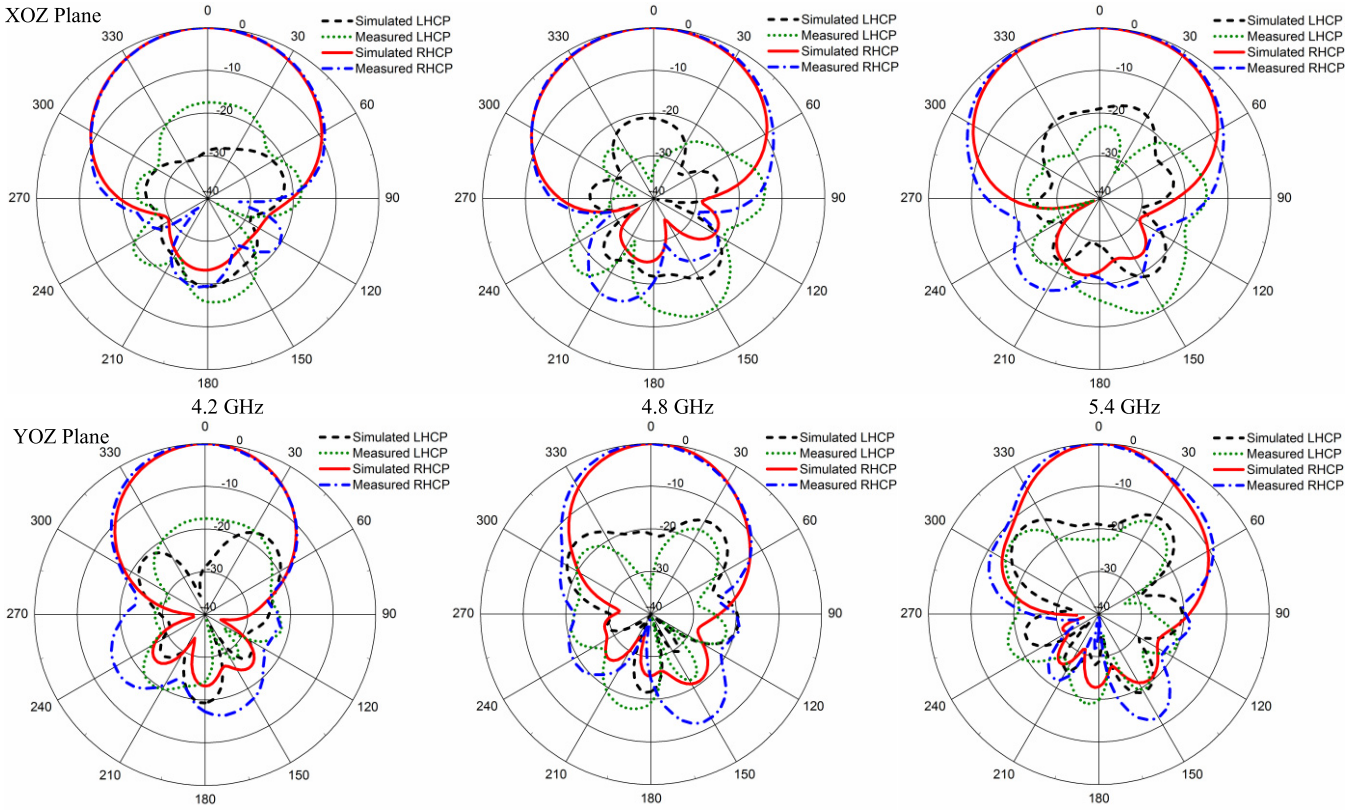
Fig. 14. Measured and simulated radiation patterns of the proposed antenna. Top row: *xoz* plane. Bottom row: *yoz* plane.

upper hemisphere. It is also noticed that the HPBW increases as the frequency goes up in the $\varphi = 0°$ plane but decreases as the frequency rises in $\varphi = 30°, 60°, 90°$ planes. According to [23], the antenna directivity is in reverse proportional to the product of HPBWs in two perpendicular planes. Although the HPBW's variation of the proposed antenna is different in each plane, the product of the HPBWs in each two perpendicular planes always increases as the frequency goes up, indicating a decrease of antenna directivity as the frequency rises, which is verified in Fig. 13.

D. Radiation Pattern and Antenna Gain

The simulated and measured antenna gain is shown in Fig. 13. As shown, the measured antenna gain is around 9–10 dBic from 4 to 5.4 GHz. Fig. 13 also shows the simulated efficiency which is larger than 90% across the whole operation bandwidth. It is indicated by the simulation that the insertion loss of the balun increases as the frequency increases, around 0.2 dB at 4 GHz and 0.8 dB at 6 GHz. It is worth pointing out that the insertion loss includes dielectric loss, conductor loss, and radiation loss. From the simulation, it is found that the radiation loss of the balun accounts for the major proportion of the insertion loss, which makes the simulated efficiency a little higher than the actual antenna radiation efficiency.

The radiation patterns of the proposed antenna at different frequency points are shown in Fig. 14. As can be seen from the figure, good agreements are observed between the simulation and measurement results of all co-pol components (RHCP) in the upper hemisphere region. The differences in the back lobe are caused by the scattering of the cable and antenna holder.

To measure the back lobe of the proposed antenna, an antenna holder is fabricated and placed above the positioner, which brings an extension of test cable and antenna holder behind the proposed antenna.

E. Comparison With Other Antennas

To demonstrate the advantages of the proposed antenna, Table II compares the proposed antenna with other reported wideband wide AR beamwidth antennas. A 3/4 turn Archimedean spiral was also simulated and compared with the proposed antenna. In order to provide a fair comparison, the spiral antenna was designed by using the same substrate that is used for the proposed antenna and the size of the spiral is adjusted to be similar physical size as the presented antenna.

Table II gives the comparison between the proposed antenna and other antennas in terms of antenna size, impedance bandwidth, AR bandwidth, and AR beamwidth. From Table II, it is shown that the proposed antenna has wider CP bandwidth and more stable AR beamwidth within the operational bandwidth. Moreover, the AR beamwidths of the proposed antenna are larger than the HPBWs in other elevation planes, which were not investigated by other researchers. The antenna can be easily extended to an antenna array which is shown in the following section.

IV. ANTENNA ARRAY AND RESULTS

A. Array Configuration

Compared with other reported wideband wide AR beamwidth CP antennas, another advantage of the proposed antenna is that it can be easily extended to an antenna array.

TABLE II

COMPARISON WITH OTHER WIDEBAND WIDE AR BEAMWIDTH ANTENNAS

|	Antenna Size (mm)	Antenna Size with Ground Plane or Cavity (mm)	Impedance Bandwidth (GHz)	3dB AR Bandwidth (GHz)	Maximum AR beamwidth and corresponding HPBW (°)	AR beamwidth vs Frequency in Main Planes	AR beamwidth in other Elevation Planes	Extension to Antenna Array
[15]	100×100×0.8, 0.53λ×0.53λ×0.004λ	Bidirectional, no ground plane	1.35-1.85, 31%	1.52-1.65, 8.2%	AR beamwidth:126° HPBW: –	—	—	—
[16]	43.7×44.8×11.5, 0.38λ×0.39λ×0.1λ	Not shown	1.85-3.38, 58.5%	2.23-2.47, 10.2%	AR beamwidth:175° HPBW:150°	—	—	—
[17]	150×150×38, 1λ×1λ×0.25λ	150×150×38, 1λ×1λ×0.25λ	1.6-2.42, 40.8%	1.63-2.27, 32.8%	AR beamwidth:85° HPBW:-	AR beamwidth=85° from 1.8 to 2.1GHz (15.4%)	—	—
[18]	76×76×0.5, 0.46λ×0.46λ ×0.003λ	120×120×30, 0.73λ×0.73λ ×0.18λ	1.27-2.36, 59.8%	1.39-1.82, 26.8%	AR beamwidth:175° HPBW: -	AR beamwidth>165° from 1.45 to 1.7GHz (15.8%)	—	—
Simulated Spiral	58.4×44.8× 0.5, 1.11λ× 0.85λ×0.01λ	90×90×18, 1.71λ×1.71λ ×0.34λ	—	5.15-6.24, 19.1%	AR beamwidth:64.2° HPBW:117°	—	AR beamwidth< HPBW	—
This Work	59.9×25.8× 0.5, 0.99λ× 0.42λ×0.008λ	90×90×18, 1.48λ×1.48λ ×0.3λ	3.4-6.5, 62.6%	4-6.15, 42%	AR beamwidth:142° HPBW:82°	AR beamwidth>100° from 4.2 to 6GHz (35.3%)	AR beamwidth> HPBW	Yes
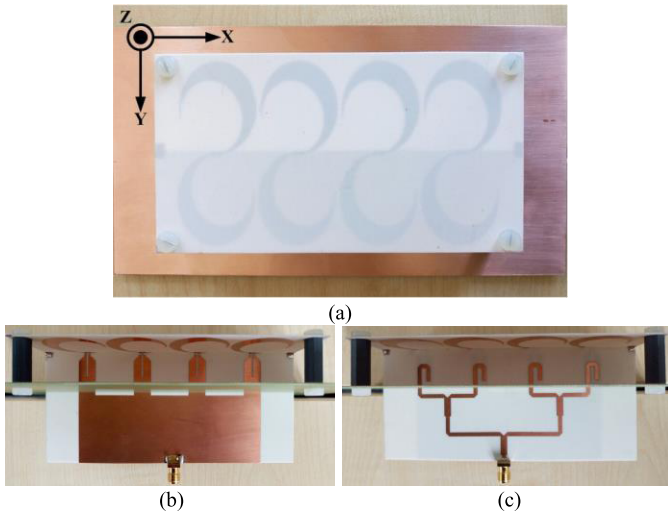
Fig. 15. Prototype of the proposed array. (a) Top view. (b) Left-side view. (c) Right-side view.

To prove this concept, a four-element linear array is designed and prototyped. Fig. 15 shows the presented antenna array, which consists of four inverted S-shaped elements. The element space is 26.5 mm which is about $0.35\lambda_0$, $0.44\lambda_0$, and $0.53\lambda_0$ for 4, 5, and 6 GHz, respectively. The small element space chosen in this design helps enhance the bandwidth of the antenna array, which is also observed in subwavelength array [24] and can be explained by the canceling of the imaginary part of mutual impedances [25]. The presented array is printed on a 0.508 mm thick Rogers RO4003C substrate with a size of 65 mm ×120 mm while a 1:4 power divider is printed on a 0.813 mm thick Rogers RO4003C substrate with a size of 60 mm × 120 mm. Below the antenna board,

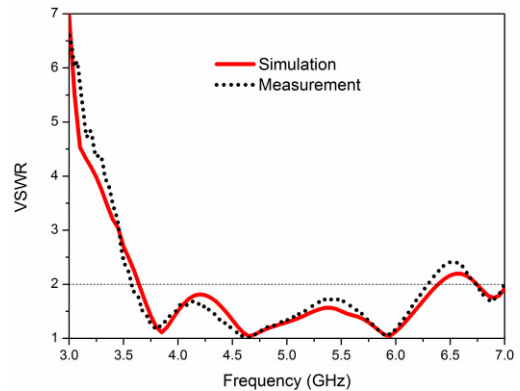Fig. 16. Simulated and measured VSWR of the proposed array.

there is a ground plane with the size of 90 mm × 165 mm. The distance between the antenna and the ground plane is kept 18 mm, which is the same as the antenna element.

It is worth pointing out that the ground plane of each balun is also kept the same size as in the antenna element. By doing this, the influence of the balun to the performance of the array can be minimized. This is because reducing the size of the ground plane of the balun effectively decreases the surface current flowing area, which makes the radiation of the balun relatively far away from the radiation region of the antenna [22].

B. VSWR and Axial Ratio Bandwidth

The comparison between the simulated and measured VSWR of the proposed array is shown in Fig. 16. As shown in the figure, the measurement result is in good agreement with the simulation result. The measured impedance bandwidth is from 3.57 to 6.3 GHz (55.3%).
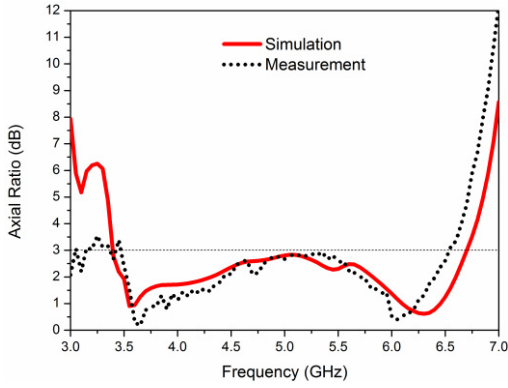
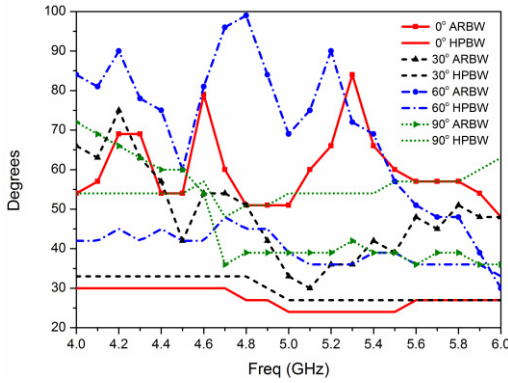Fig. 17. Simulated and measured AR of the proposed array.

Fig. 18. Measured AR beamwidths and HPBWs of the array.

The simulated and measured AR of the presented array is shown in Fig. 17. The measured CP bandwidth (AR < 3 dB) of the presented array is from 3.5 to 6.5 GHz (60%).

C. Axial Ratio Beamwidth of the Array

To evaluate the AR beamwidth characteristics of the array, Fig. 18 shows the measured AR beamwidths and HPBWs in planes $\varphi = 0°$, $30°$, $60°$, $90°$. As shown, the AR beamwidths are larger than the HPBWs from 4 to 6 GHz in elevation planes $\varphi = 0°$, $30°$, $60°$. However, the AR beamwidth is smaller than the HPBW in plane $\varphi = 90°$, which may due to the narrow AR beamwidth of the antenna element in this plane and the effect of mutual coupling between each element.

D. Radiation Pattern and Gain

To evaluate the radiation performance of the presented array, radiation patterns of the proposed array at 4 and 6 GHz are shown in Fig. 19. As shown, the measurement results agree well with the simulation results. Better agreements are obtained due to the fact that the array has a larger ground plane which provides better shielding to the cables and antenna holder which are placed behind the antenna during the measurement.

Fig. 20 shows the measured and simulated gain of the presented antenna array. As shown, the measured gain is around 12–14 dBic from 4 to 6 GHz. The simulated insertion loss of the array feeding network is around 0.5–1.2 dB from 4 to 6 GHz. The difference of the gain between the array and
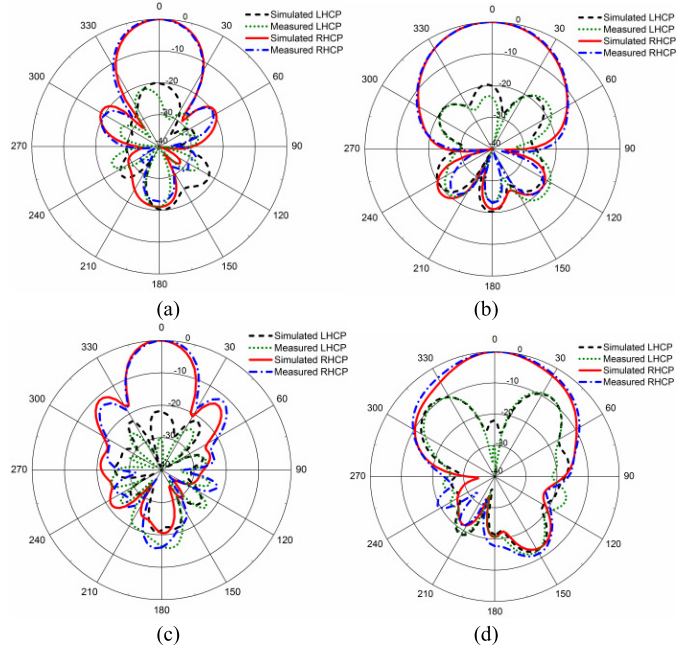

Fig. 19. Simulated and measured radiation patterns of the proposed array. (a) 4 GHz *xoz* plane. (b) 4 GHz *yoz* plane. (c) 6 GHz *xoz* plane. (d) 6 GHz *yoz* plane.
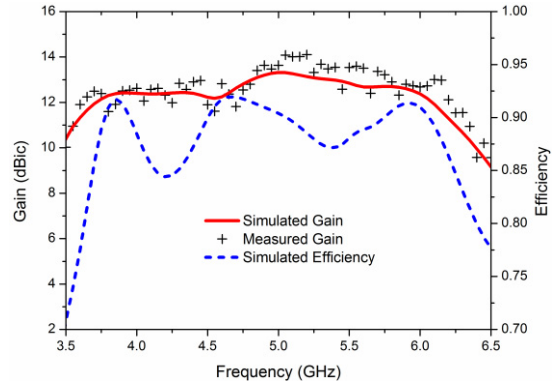

Fig. 20. Gain and simulated efficiency of the antenna array.

the antenna element increases as frequency goes higher, which mainly attributes to the decreased mutual coupling at higher frequencies. Besides, the increase of the ground plane size has some effect on the antenna gain as well. The simulated efficiency of the antenna array, as shown in Fig. 20, is larger than 85% from 4 to 6 GHz.

V. CONCLUSION

A wideband CP antenna with wide AR beamwidth within its operational bandwidth is presented in this paper. The proposed inverted-S antenna achieves a CP bandwidth of 42% and over 140° AR beamwidth, leading to a wider CP bandwidth compared with other reported wide AR beamwidth CP antennas. Besides, the AR beamwidths of the presented antenna are larger than the HPBWs in other elevation planes. Due to its simple configuration, the presented antenna could be easily extended to an array antenna with 60% CP bandwidth. Owing to these advantages, the proposed antenna is promising for the applications in GNSS systems and wide-angle CP beam-scanning arrays.

REFERENCES

[1] S. Gao, Q. Luo, and F. Zhu, *Circularly Polarized Antennas*. Hoboken, NJ, USA: Wiley, 2013.

[2] H. Iwasaki, "A circularly polarized small-size microstrip antenna with a cross slot," *IEEE Trans. Antennas Propag.*, vol. 44, no. 10, pp. 1399–1401, Oct. 1996.

[3] Y.-X. Guo, K.-W. Khoo, and L. C. Ong, "Wideband circularly polarized patch antenna using broadband baluns," *IEEE Trans. Antennas Propag.*, vol. 56, no. 2, pp. 319–326, Feb. 2008.

[4] R. B. Waterhouse, "Stacked patches using high and low dielectric constant material combinations," *IEEE Trans. Antennas Propag.*, vol. 47, no. 12, pp. 1767–1771, Dec. 1999.

[5] J. Wu, Y. J. Cheng, and Y. Fan, "Millimeter-wave wide band high-efficiency circularly polarized planar array antenna," *IEEE Trans. Antennas Propag.*, vol. 64, no. 2, pp. 535–542, Feb. 2016.

[6] M. Li and K.-M. Luk, "A wideband circularly polarized antenna for microwave and millimeter-wave applications," *IEEE Trans. Antennas Propag.*, vol. 62, no. 4, pp. 1872–1879, Apr. 2014.

[7] J. J. H. Wang, "Antennas for global navigation satellite system (GNSS)," *Proc. IEEE*, vol. 100, no. 7, pp. 2349–2355, Jul. 2012.

[8] X. Bai, S.-W. Qu, S. Yang, J. Hu, and Z.-P. Nie, "Millimeter-wave circularly polarized tapered-elliptical cavity antenna with wide axial-ratio beamwidth," *IEEE Trans. Antennas Propag.*, vol. 64, no. 2, pp. 811–814, Feb. 2016.

[9] Nasimuddin, X. Qing, and Z. N. Chen, "A compact circularly polarized slotted patch antenna for GNSS applications," *IEEE Trans. Antennas Propag.*, vol. 62, no. 12, pp. 6506–6509, Dec. 2014.

[10] Nasimuddin, Y. Anjani, and A. Alphones, "A wide-beam circularly polarized asymmetric-microstrip antenna," *IEEE Trans. Antennas Propag.*, vol. 63, no. 8, pp. 3764–3768, Aug. 2015.

[11] K. B. Ng, C. H. Chan, and K. M. Luk, "Low-cost vertical patch antenna with wide axial-ratio beamwidth for handheld satellite communications terminals," *IEEE Trans. Antennas Propag.*, vol. 63, no. 4, pp. 1417–1424, Apr. 2015.

[12] S. X. Ta, H. Choo, I. Park, and R. W. Ziolkowski, "Multi-band, wide-beam, circularly polarized, crossed, asymmetrically barbed dipole antennas for GPS applications," *IEEE Trans. Antennas Propag.*, vol. 61, no. 11, pp. 5771–5775, Nov. 2013.

[13] S. L. Zuo, L. Yang, and Z. Y. Zhang, "Dual-band cp antenna with a dual-ring cavity for enhanced beamwidth," *IEEE Antennas Wireless Propag. Lett.*, vol. 14, pp. 867–870, 2015.

[14] X. L. Bao and M. J. Ammann, "Dual-frequency dual circularly-polarised patch antenna with wide beamwidth," *Electron. Lett.*, vol. 44, no. 21, pp. 1233–1234, Oct. 2008.

[15] Y. Luo, Q. X. Chu, and L. Zhu, "A low-profile wide-beamwidth circularly-polarized antenna via two pairs of parallel dipoles in a square contour," *IEEE Trans. Antennas Propag.*, vol. 63, no. 3, pp. 931–936, Mar. 2015.

[16] H. Jiang, Z. Xue, W. Li, and W. Ren, "Broad beamwidth stacked patch antenna with wide circularly polarised bandwidth," *Electron. Lett.*, vol. 51, no. 1, pp. 10–12, 2015.

[17] K. M. Mak and K. M. Luk, "A circularly polarized antenna with wide axial ratio beamwidth," *IEEE Trans. Antennas Propag.*, vol. 57, no. 10, pp. 3309–3312, Oct. 2009.

[18] S. X. Ta and I. Park, "Crossed dipole loaded with magneto-electric dipole for wideband and wide-beam circularly polarized radiation," *IEEE Antennas Wireless Propag. Lett.*, vol. 14, pp. 358–361, 2015.

[19] D. Yu, S.-X. Gong, Y.-T. Wan, Y.-L. Yao, Y.-X. Xu, and F.-W. Wang, "Wideband omnidirectional circularly polarized patch antenna based on vortex slots and shorting vias," *IEEE Trans. Antennas Propag.*, vol. 62, no. 8, pp. 3970–3977, Aug. 2014.

[20] K.-F. Hung and Y.-C. Lin, "Novel broadband circularly polarized cavity-backed aperture antenna with traveling wave excitation," *IEEE Trans. Antennas Propag.*, vol. 58, no. 1, pp. 35–42, Jan. 2010.

[21] P. S. Hall, J. S. Dahele, and J. R. James, "Design principles of sequentially fed, wide bandwidth, circularly polarised microstrip antennas," *IEE Proc. H-Microw., Antennas Propag.*, vol. 136, no. 5, pp. 381–389, Oct. 1989.

[22] R. Bawer and J. J. Wolfe, "A printed circuit balun for use with spiral antennas," *IRE Trans. Microw. Theory Techn.*, vol. 8, no. 3, pp. 319–325, May 1960.

[23] C. A. Balanis, *Antenna Theory: Analysis and Design*, vol. 1. Hoboken, NJ, USA: Wiley, 2005.

[24] D. M. Pozar, "Wideband reflectarrays using artificial impedance surfaces," *Electron. Lett.*, vol. 43, pp. 1–2, Feb. 2007.

[25] B. A. Munk, *Finite Antenna Arrays and FSS*. Hoboken, NJ, USA: Wiley, 2003.
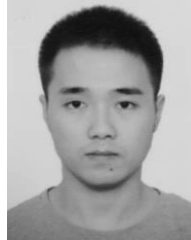
Long Zhang received the B.S. and M.S. degrees in electrical engineering from the Huazhong University of Science and Technology (HUST), Wuhan, China, in 2009 and 2012, respectively. He is currently pursuing the Ph.D. degree with the University of Kent, Canterbury, U.K.

He was an Antenna Engineer with Huawei, Wuhan, China, in 2012 and then a Graduate Research Assistant with the Multi-Spectral Information Processing Laboratory, HUST, in 2013. His current research interests include circularly polarized antennas and arrays, smart antennas, reconfigurable antennas, mobile terminal antennas, and reflectarray.

Steven Gao (M'01–SM'16) received the Ph.D. degree in microwave engineering from Shanghai University, Shanghai, China, in 1999.

He is currently a Professor and Chair of RF and Microwave Engineering with the University of Kent, Canterbury, U.K. He has co-authored two books, including *Space Antenna Handbook* (Wiley, 2012) and *Circularly Polarized Antennas* (IEEE-Wiley, 2014), published more than 250 papers, and holds several patents in smart antennas and RF. His current research interests include smart antennas, phased arrays, satellite antennas, RF/microwave/mm-wave/THz circuits, satellite communications, UWB radars, synthetic-aperture radars, and mobile communications.

Qi Luo (S'08–M'12) is a Research Associate with the University of Kent, Canterbury, U.K.

Paul R. Young (M'00–SM'05) is a Senior Lecturer with the University of Kent, Canterbury, U.K.
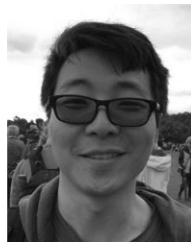
Wenting Li received the B.S. degree in electronic information engineering and the M.S. degree in electromagnetic field and microwave technology from Northwestern Polytechnical University, Xi'an, China, in 2011 and 2014, respectively. He is currently pursuing the Ph.D. degree with the University of Kent, Canterbury, U.K.

His current research interests include reflectarray antennas, reconfigurable antennas, circularly polarized antennas, and multibeam antennas.

Qingxia Li (M'08) is a Professor with Huazhong University of Science and Technology, Wuhan, China.